PAPER • OPEN ACCESS

Synthesis of praseodymium-and molybdenum-sulfide nanoparticles for dye-photodegradation and near-infrared deep-tissue imaging

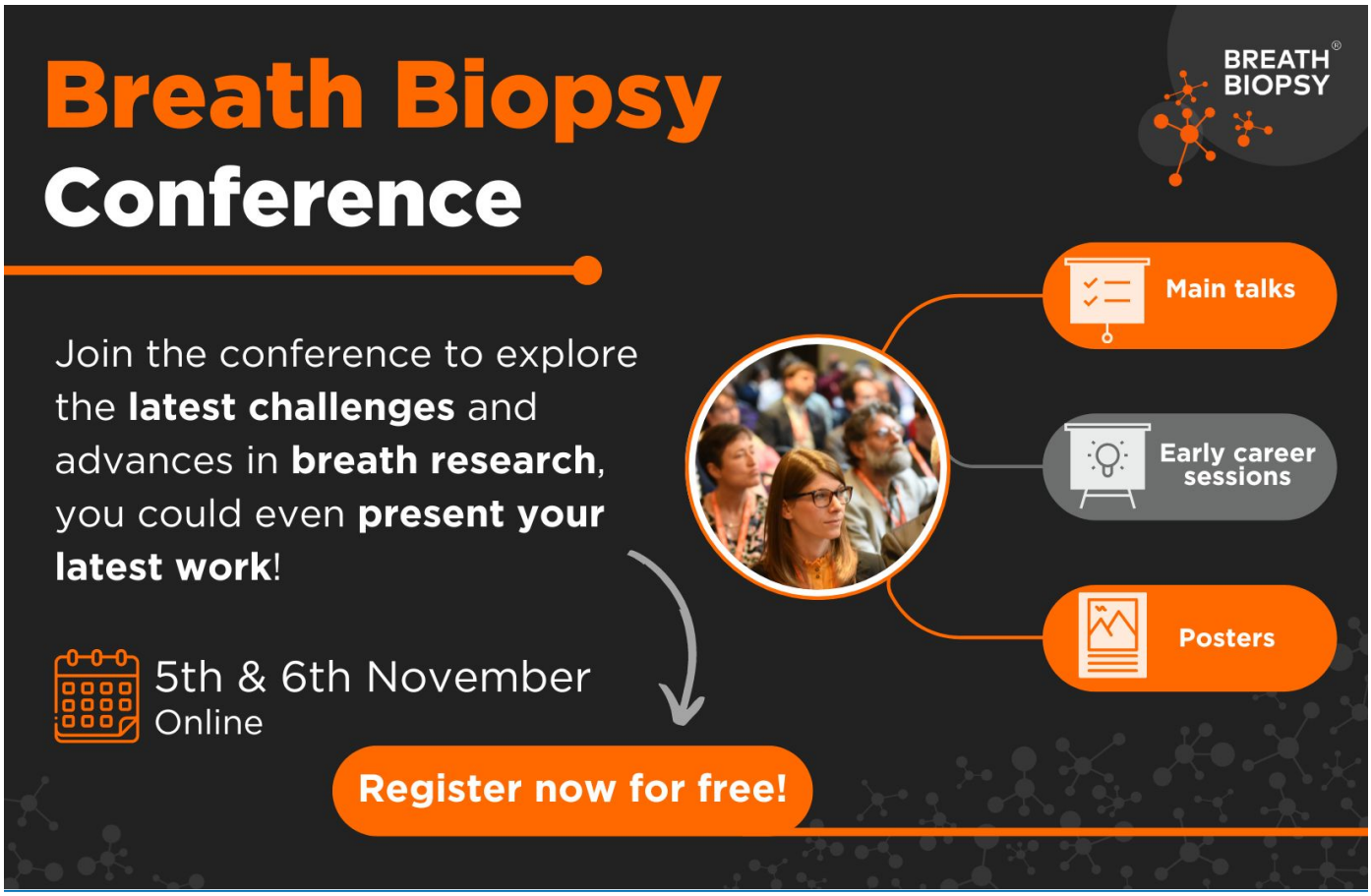

Materials Research Express

PAPER

Synthesis of praseodymium-and molybdenum- sulfide nanoparticles for dye-photodegradation and near-infrared deep-tissue imaging

Ye Wu[1], **Pengfei Ou**[2], **Jun Song**[2], **Ling Zhang**[3], **Yingcheng Lin**[3,4,7], **Pengfei Song**[5,7] **and Jian Xu**[6,7]

[1] School of Electrical and Automation Engineering, Jiangsu Key Laboratory of 3D Printing Equipment and Manufacturing, Nanjing Normal University, Nanjing,210046, People's Republic of China
[2] Department of Mining and Materials Engineering, McGill University, Montreal, QC H3A 0C5, Canada
[3] College of Microelectronics and Communication Engineering, Chongqing University, Chongqing 400044, People's Republic of China
[4] Key Laboratory of Dependable Service Computing in Cyber Physical Society of Ministry of Education, Chongqing University, Chongqing 400044, People's Republic of China
[5] Department of Electrical and Electronic Engineering, Xi'an Jiaotong-Liverpool University, Suzhou, Jiangsu 215123, People's Republic of China
[6] Division of Electrical and Computer Engineering, Louisiana State University, Baton Rouge, Louisiana 70803, United States of America
[7] Authors to whom any correspondence should be addressed.

E-mail: linyc@cqu.edu.cn, pengfei.song@xjtlu.edu.cn **and** jianxu1@lsu.edu

Keywords: near-infrared fluorescence, deep tissue imaging, dye-photodegradation, fluorescein sodium salt

Supplementary material for this article is available online

OPEN ACCESS

RECEIVED
27 December 2019

REVISED
8 March 2020

ACCEPTED FOR PUBLICATION
19 March 2020

PUBLISHED
30 March 2020

Abstract

Development of nanoparticles with multi-functionalities is of great importance. In this study, praseodymium sulfide (Pr_2S_3) and molybdenum sulfide (MoS_2) nanoparticles were synthesized. The structural, morphological and optical properties of the as-obtained products were investigated by XRD, XPS, TEM, UV–vis-NIR spectroscopy, and photoluminescence spectroscopy. Pr_2S_3 is found to be used in selective photodegradation of fluorescein sodium salt. MoS_2 can be utilized for selective photodegradation of rhodamine B. In the mixture of rhodamine B, fluorescein sodium salt and rhodamine 6 G, most of rhodamine B and part of fluorescein sodium salt are optically degraded by Pr_2S_3. In the mixture of rhodamine B, fluorescein sodium salt and rhodamine 6 G, part of fluorescein sodium salt and most of rhodamine B is degraded by MoS_2. Moreover, they emit near-infrared fluorescence (800–1100 nm) when excited by the 785 nm light. Deep tissues imaging with high-contrast is shown, utilizing a nanoparticle-filled centrifuge tube covered with animal tissues (pig Bacon meat). Maximum imaging depth below the tissue surface of 1 cm is achieved. Our work provides a rapid yet efficient procedure to make nanoparticles for dual-application-potential in dye-photodegradation and near-infrared deep tissue imaging.

1. Introduction

Dyeing is widely utilized in textile plants for coloring clothes. Much attention should be paid to the issue that streams are facing grave problems because of the discharge of color wastewater from factories. It creates a severe environment for fish due to the toxicity of dyes existing in the wastewater. It is worth noting that dyes usually contain a synthetic origin and complex aromatic molecular structures. This makes them very stable and difficult to degrade. It is important to perform dye-pretreatment for the wastewater given that these dye materials would flow into our drinking water pipes if the wastewater wasn't treated properly in the very beginning. Taking the aspect of environmental issue into account, the research activities about dye degradation are active [1–10]. One effective way for dye-pretreatment can be using photodegradation. More importantly, it is considered to be a green technology when organic pollutants are degraded under solar light or white light irradiation [1–10]. Praseodymium- and molybdenum- based material systems show their potentials for photodegradation of

organic materials. Several examples can be found in photodegradation of methylene blue [1], rhodamine B [2], 2-naphthol [3], 2,4-dichlorophenol[4], methyl orange[5], nitrobenzene [6] and Eriochrome Black T [7], via Pr, N co-doped TiO_2 [1], $PrFeO_3$ [2], Pr_6O_{11} [3], Pr doped $Bi_2Sn_2O_7$ [4], $CuFe_{2-x}Pr_xO_4$ [5], Pr:Y_2SiO_5 [6] and Pr doped ZnO [7], respectively. Moreover, it is reported that Reactive Black 5 [8], methylene blue/rhodamine B/methyl orange [9], can be optically degraded by MoS_2 [8] and $MoSe_2$ [9].

Furthermore, MoO_3 is useful for the photodegradation of methylene blue [10]. These research endeavors inspire us that constructing materials based on Pr or Mo based entities can be effective for introducing photodegradation of the dyes. The making of nanoparticles to fulfill multiple tasks is of great interest, given that it can lower the cost in practical applications.

While the dye-photodegradation is one functionality of the materials that we are looking for, we still look for other potential applications.

Clinic practices involve with activities to perform inspection below tissue surface in order to find out the structure and function of the organs via using optical microscopy. It could be noted that deep tissue imaging of biological tissues is important for clinical applications. It helps doctors to acquire critical information of patients. Based on the imaging results, the doctors can decide the following treatment for the diseases.

However, there are many complex organic components existing in biological tissues, leading to strong optical absorption/scattering at specific wavelength region. It should be mentioned that light scattering generally exists on those spots under tissue surface. It lowers the imaging qualities, which makes the organs very difficult to be identified.

In order to overcome the obstacle of scattering tissues, one possible method is performing the imaging within near-infrared (NIR) window (750–1100 nm), which is superior comparing with the ultraviolet-visible region. It can improve imaging quality vastly since it involves with the using of fluorophores emitting and the achieving of low levels of photon absorption [11–16].

Therefore, in practical fluorescence imaging of the biological tissues, materials that process near infrared optical emission can be favorable. Their long-wavelength fluorescence can penetrate the thickness of the tissue and reach the imaging camera. These materials are very useful in deep -tissue imaging.

In the present study, praseodymium sulfide (Pr_2S_3) and molybdenum sulfide (MoS_2) nanoparticles were synthesized. The structural, morphological and optical properties of the as-obtained products were characterized by x-ray diffraction (XRD), x-ray photoelectron spectroscopy (XPS), transmission electron microscopy (TEM), ultraviolet-visible-near-infrared (UV–vis-NIR) absorption spectroscopy, and photoluminescence spectroscopy. Three different dyes (rhodamine B, rhodamine 6 G and fluorescein sodium salt) are tested for photodegradation effect. It is found that Pr_2S_3 can be used for photodegradation of fluorescein sodium salt while MoS_2 can be used for photodegradation of rhodamine B. Furthermore, they present NIR fluorescence (800–1100 nm) upon the 785 nm light excitation. Their deep-tissue imaging function is demonstrated, using a nanoparticle-loaded 2 ml centrifuge tube covered with animal tissues (pig Bacon meat). Maximum imaging depth below the tissue surface of 1 cm can be achieved. Our work shows the making of nanoparticles for dual applications in dye-photodegradation and NIR deep-tissue imaging.

2. Experimental

2.1. Materials

Fumaric acid, 2-methylimidazole, dimethylsulfoxide, L-cysteine, sulfuric acid, praseodymium (III,IV) oxide, molybdenum(VI) oxide, ethanol, rhodamine B, rhodamine 6 G and fluorescein sodium salt were all purchased from Alfa Aesar.

2.2. Preparation of precursors containing Pr and Mo

Praseodymium oxide (Pr_2O_3, 5 g) and sulfuric acid (85% , 20 ml) were mixed and stirred, then deionized water (50 ml) were added drop by drop. The acquired solution was heated with the temperature of 100 °C to get a clear Solution 1.

Molybdenum dioxide (MoO_2, 5 g) and sulfuric acid (85%, 40 ml) were mixed and stirred, then deionized water (20 ml) were added dropwise. The acquired solution was heated with the temperature of 100 °C to get a clear Solution 2.

2.3. Preparation of organic precursors

Three types of organic solutions were prepared.

Solution 3 was made by dissolving 2-methylimidazole (2 g), terephthalic acid (5 g), fumaric acid (5 g), D(+)-glucose (5 g), oxalic acid dehydrate (5 g) in dimethylformamide (200 mL).

Solution 4 was prepared by mixing dimethyl sulfoxide (50 mL), oleic acid (40 ml), triethylamine (40 ml), diethylene glycol (40 ml), dimethyl sulfoxide (20 ml) and methacrylic an hydride (10 ml).

Solution 5 was done by dissolving L-cysteine (2 g) in de-ionized water (50 ml).

Then Solution 3, Solution 4 and Solution 5 were mixed, some light yellow precipitate appeared. The mixture solution was stirred for 2 h to get a clear solution (Solution 6).

2.4. Preparation of Pr_2S_3 nanoparticles

Solution 1 (20 ml) was mixed with Solution 6 (80 ml). The mixture was stirred speedily for 2 h to get Solution 7. Solution 7 was firstly centrifuged with a speed of 6000 RPM for 0.5 h, then 10000 RPM for 0.5 h, followed by 14000 RPM for 0.5 h to get the final Pr_2S_3 nanoparticles.

2.5. Preparation of MoS_2 nanoparticles

The preparation of MoS_2 nanoparticles is similar to that of Pr_2S_3 nanoparticles. The only difference is the using of Solution 2 instead of Solution 1.

2.6. Preparation of several dye solutions

Preparation of dye solution FSS: Fluorescein sodium salt (0.1 g) was dissolved in deionized water (50 ml) to get the solution FSS.

Preparation of dye solution R6G: Rhodamine 6G (0.1 g) was dissolved in ethanol (50 ml) to get the solution R6G.

Preparation of dye solution RB: Rhodamine B (0.53 g) was dissolved in deionized water (100 ml) to get the solution RB.

Preparation of dye solution Dye 1: FSS (2 ml), RB (500 μl) and R6G (500 μl) was mixed and stirred to get the solution Dye 1.

Preparation of dye solution Dye 2: FSS (500 μl), RB (2 ml) and R6G (500 μl) was mixed and stirred to get the solution Dye 2.

2.7. Setup for photodegradation

A Halogen light bulb (Model: Double Ended Quartz FCL, OSRAM) with maximum output optical power 500 W is utilized for generating white light. The output optical power of the light bulb can be adjusted by a self-built controller.

The dye solutions prepared in section 2.6 were mixed with Pr_2S_3 or MoS_2 nanoparticles.

The white light from the Halogen light bulb was shining on a glass tube filled with the mixture of Pr_2S_3 or MoS_2 nanoparticles and the dye solutions.

The dye solutions would change the color due to the photodegradation effect introduced by the nanoparticles. After photodegradation test was done in 30 min, the acquired dye solutions were collected for optical spectroscopy study.

2.8. Characterization

The XPS data was collected via a K-Alpha XPS instrument (Thermo Scientific). Powder XRD data was got from a PANalytical Empyrean XRD instrument. The XRD profile simulation and crystal structure derivation were done through a GSAS/DRAWxtl V5.5 software package. TEM images were obtained through a JEOL 1400 TEM (120 kV). The UV–vis-NIR absorption and UV–vis fluorescence spectroscopy were acquired through a SPARK optical spectrometer.

2.9. Setup of NIR fluorescence measurement

A self-built fluorescence measurement setup is utilized for collecting NIR fluorescence from the samples. A laser diode (Thorlab Inc.) provided the excitation light with the center wavelength of 785 nm. One optical fiber bundle was used as delivering the excitation light. Another optical fiber bundle was applied for collection of the fluorescence. They were combined in a probe, which was moved around the surface of the sample to collect the fluorescence. An NIR long-pass filter (Thorlab Inc.) was applied to get rid of the excitation light since the excitation light can be collected by the optical fiber bundle. The collected fluorescence was focused on a spectrometer (Ocean Optics).

2.10. Setup of NIR deep-tissue imaging setup

A 785 nm laser is used as an excitation light source. An optical fiber bundle is utilized to deliver the optical power. When the sample surface is shined by the laser, NIR fluorescence can emit from the sample surface. The image of the sample can be captured by a near infrared camera which is seating above the sample. Here, a

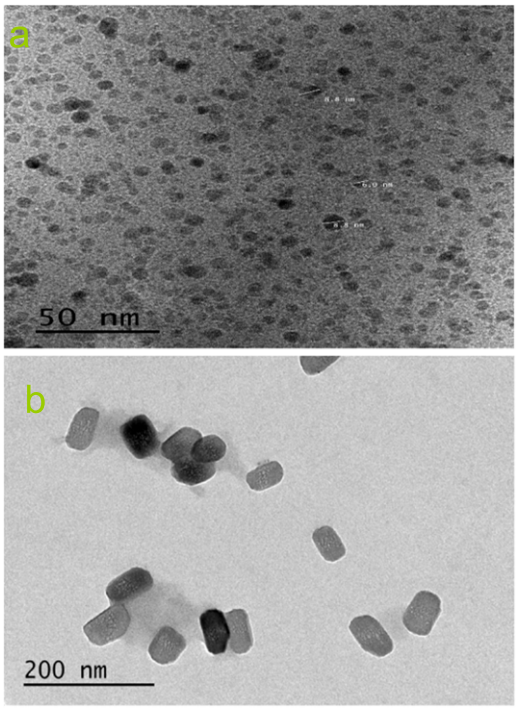

Figure 1. TEM images of the nanoparticles: (a) Pr_2S_3; (b)MoS_2.

centrifuge tube filled with Pr_2S_3 or MoS_2 nanoparticles in ethanol (2 ml) solution was used the imaging object. The centrifuge tube with first put in the position around the NIR camera to capture a control image. Then the centrifuge tube was covered with one layer of Bacon meat. The NIR camera was used to check the image of the centrifuge tube. Although the Bacon meat can block some of the NIR fluorescence emitting from the nanoparticles, some of the strong NIR fluorescence are able to penetrate through the Bacon meat and reach the NIR camera.

3. Results and discussion

3.1. XRD/TEM/XPS study

The XRD profiles were analyzied, which were confirmed as the phases of Pr_2S_3 and MoS_2. The XRD profiles can be found in figures S1 and S2 in supportive information is available online at stacks.iop.org/MRX/7/036203/mmedia.

TEM was used to find out the morphology and size of the nanoparticles (see figures 1(a)–(b)). The Pr_2S_3 nanoparticles show spherical shape. The MoS_2 nanoparticles present rectangular shape. The nanoparticle size distribution is shown in figure S3 in supportive information.

XPS was applied to study the core levels, valence band and chemical bonding information of the samples.

Figures 2(a)–(b) show the XPS high scanning spectra for Pr_2S_3. Pr 3d spectra (figure 2(a)) reveal peaks at 933.3 eV, 943.6 eV, 953.9 eV and 964.3 eV. The 933.3 eV and 953.9 eV peaks are attributed to the main peaks of Pr $3d_{5/2}$ and Pr $3d_{3/2}$. The other two peaks at 943.6 eV and 964.3 eV (denoted as 'A ' and ' B' in figure 2(a)) are considered as the satellite peaks, which is caused by the effect of the covalency hybridization as well as the multiplet effect associated with some modification of the spectral shape and broadening [17, 18]. The deconvolution of S 2p spectra (figure 2(b)) present peaks at 167.9 eV and 168.9 eV, which are assigned to S-Pr bonding and S-S-Pr bonding, respectively [19–21].

Figures 3(a)–(b) present the XPS high scanning spectra for MoS_2. Figure 3(a) depicts the Mo 3d spectra, which present peaks at 231.1 eV, 232.2 eV, 234.3 eV and 235.3 eV. The 232.2 eV and 235.3 eV peaks are assigned to the core levels of Mo $3d_{5/2}$ and Mo $3d_{3/2}$, separately [22]. The 231.1 eV and 234.3 eV peaks are considered as satellite peaks. S 2p spectra are depicted in figure 3(b), which presents peaks at 167.6 eV and 168.6 eV. The 167.6 eV peak is assigned to S-Mo bonding. The 168.6 eV peak is considered as the effect of S-S-Mo bonding [19–21].

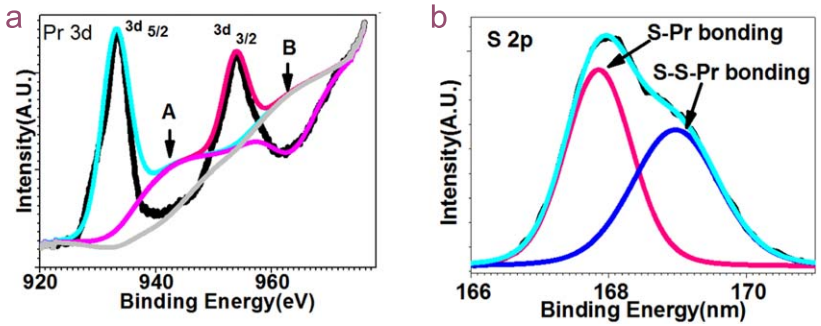

Figure 2. XPS high scanning spectra for Pr_2S_3: (a) Pr 3d; (b) S 2p.

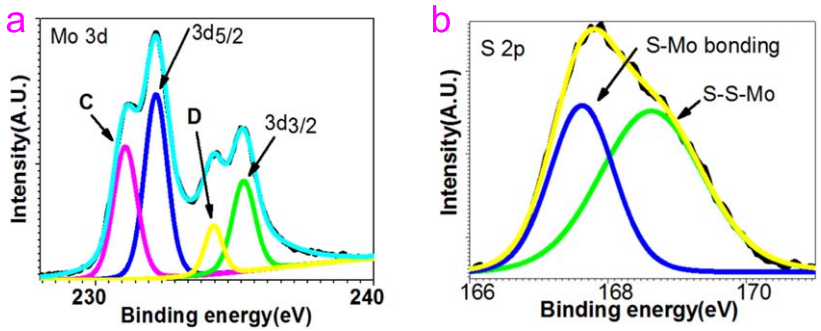

Figure 3. XPS high scanning spectra for MoS_2: (a) Mo 3d; (b) S 2p.

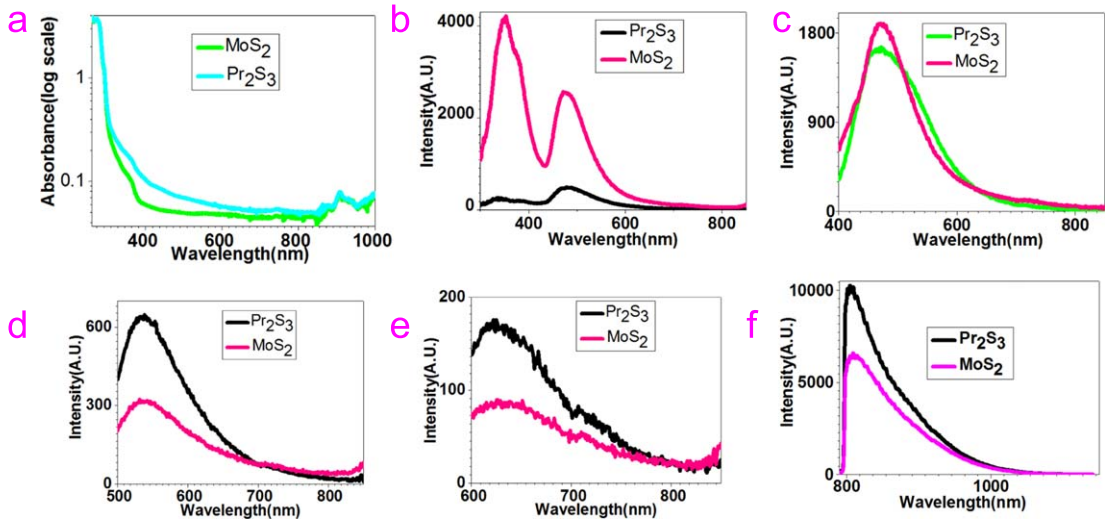

Figure 4. (a) Optical absorption. Fluorescence excited by the light with different wavelengths: (b) 280 nm light; (c) 380 nm light; (d) 480 nm light; (e) 580 nm light; (f) 785 nm light.

3.2. Optical property

The studies of optical absorption and fluorescence were done for better understanding of the samples. Figures 4(a)–(f) plot the optical absorption and fluorescence generated by various light sources. The absorption spectra (see figure 4(a)) for both samples show a shoulder around 260–380 nm and a major absorption peak around 907 nm. The absorption of Pr_2S_3 is higher than MoS_2 in the ultraviolet-visual light range (around 298 nm-750 nm).

Both samples show polychromatic-photoluminescence upon 280 nm, 380 nm, 480 nm, 580 nm and 785 nm light excitation (figures 4(b)–(f)). The fluorescence intensities of MoS_2 generated by 280 nm, 380 nm and 480 nm light of MoS_2 are higher than those of Pr_2S_3. However, the fluorescence intensities of MoS_2 generated by

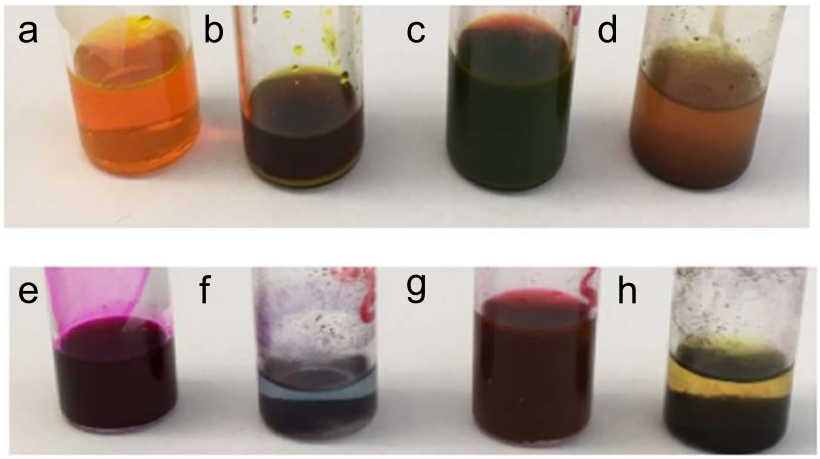

Figure 5. The photodegradation changes the color of the dye and dye mixture in the bottles. a: Fluorescein sodium salt solution without any photodagradation treatment. b: Fluorescein sodium salt solution without photodagradation treatment after photodegradation treatment via Pr_2S_3 nanoparticles. c: Dye 1 solution without any photodagradation treatment. d: Dye 1 solution after photodegradation treatment via Pr_2S_3 nanoparticles. e: Rhodamine B solution without photodegradation treatment. f: Rhodamine B solution after photodegradation treatment via MoS_2 nanoparticles. g: Dye 2 solution without photodegradation treatment. h: Dye 2 after photodegradation treatment via MoS_2 nanoparticles. Here, Dye1 and Dye 2 are made by the mixture of rhodamine B, rhodemaine 6 G and fluorescein sodium salt (see the ' Experimental' section for detail preparation).

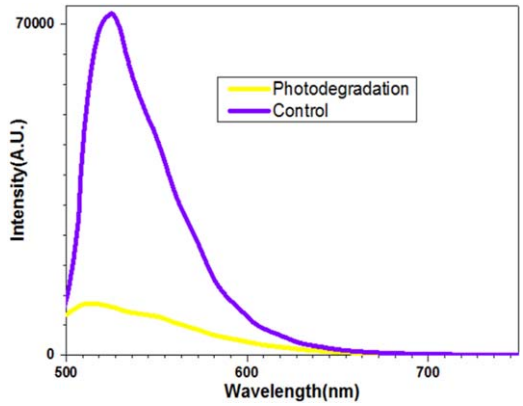

Figure 6. Pr_2S_3 can be used for photodegradation treatment of fluorescein sodium salt under white light irradiation. The purple curve is the original fluorescence of fluorescein sodium salt excited by the 440 nm light (the 'Control'). After optical degradation treatment via Pr_2S_3 nanoparticle, the intensity of the fluorescence is significantly decreased (the yellow curve).

580 nm and 785 nm light are lower than those of Pr_2S_3. Upon 785 nm light excitation, both samples show NIR fluorescence covering from 794.06 nm to 1143.60 nm. The fluorescence spectra show a peak at 808 nm. This can be used for the purpose of NIR deep-tissue image which will be discussed later.

3.3. Photodegradation of dyes

Figure 5 shows the photodegradation test of dye through Pr_2S_3 and MoS_2 nanoparticles. The photodegradation changes the color of the dye or dye mixture in the bottles of a, b, c, d, e, f, g and h. Bottle a is filled with the fluorescein sodium salt solution without any treatment of the photodegradation, whose color is yellow.

After photodegradation treatment via Pr_2S_3 nanoparticles, its color is changed to be dark grey (see Bottle b in figure 5). Figure 6 clearly presents the change of fluorescence spectra after photodegradation test. Fluorescence spectra of Bottle a show a strong peak at 525.18 nm when excited by 440 nm light (purple curve in figure 6). The fluorescence intensity of Bottle b excited by 440 nm light drops dramatically and the peak shifts to 515.78 nm (see yellow curve in figure 6). The photodegradation effect of dye mixture is also investigated. Bottle c in figure 5 is filled with Dye 1, which is the dye mixture of rhodamine B, rhodemaine 6 G and fluorescein sodium salt.

Its color is dark red. Clearly, the photodegradation treatment with Pr_2S_3 nanoparticles changes its color to light yellow (see Bottle d in figure 5). Figure 7(a) presents fluorescence of Bottle c and d in figure 5 excited by 440 nm light. The fluorescence of Bottle c reveals two major peaks at 524.08 nm and 575 nm. The fluorescence of Bottle d only shows one peak at 515.38 nm. It should be noted that Pr_2S_3 nanoparticles have been filled into the

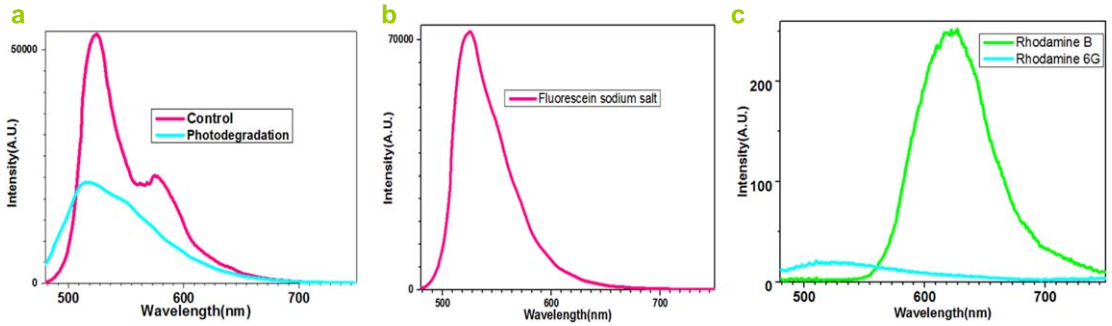

Figure 7. (a) The fluorescence spectra of the dye mixture (Dye 1) excited by 440 nm light are examined. Pink curve: the 'Control' (no photodegradation treatment is applied); Cyan curve: after photodegradation treatment via Pr_2S_3 nanoparticles. (b) The fluorescence of fluorescein sodium salt excited by 440 nm light. (c) The fluorescence spectra of rhodamine B and rhodamine 6 G excited by 440 nm.

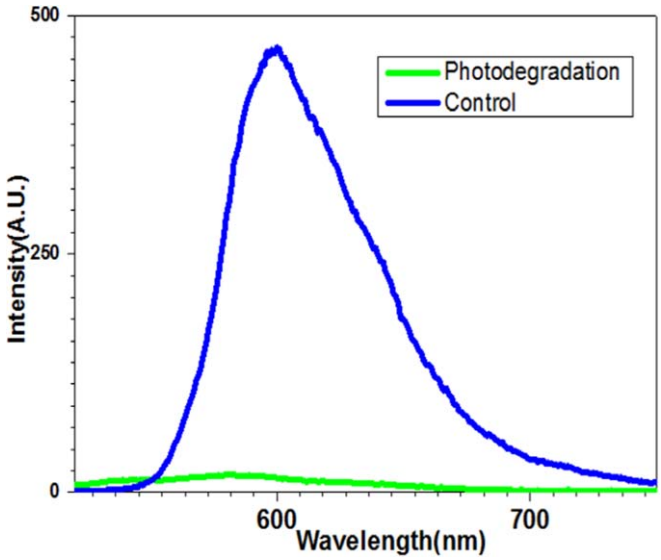

Figure 8. MoS_2 can be used for optical degradation of rhodamine B. The blue curve is the original fluorescence of rhodamine B excited by the 480 nm light (the 'control'). After optical degradation treatment via MoS_2 nanoparticles, the intensity of the fluorescence is significantly suppressed.

three bottles which contain rhodamine 6 G, rhodamine B and fluorescein sodium salt separately for photodegradation test. It is found that Pr_2S_3 can be selectively to degrade the fluorescein sodium. However, when these three kinds of dyes were mixed together (see Bottle c in figure 5), not only the fluorescein sodium salt but also the rhodamine B was degraded. As show in the bottle d in figure 5, no red color (introduced by the rhodamine B) is observed. This is also supported by the fluorescence spectra analysis. Figures 7(b) and (c) present the fluorescence spectra of rhodamine B, rhodemaine 6 G and fluorescein sodium salt excited by 440 nm light. It can be found that the rhodamine B spectra show a red light peak at 623.5 nm; the rhodamine 6 G spectra show a green light peak at 521. 65 nm; the fluorescein sodium salt spectra show a green light peak at 524.6 nm. Interestingly, in figure 7(a), there is only one green light peak at 515.4 nm left, which may be due to the combination effect of the fluorescein sodium salt and the rhodamine 6 G. The peak at 623.5 nm generated from the rhodamine B is absent. It indicates that most of the rhodamine B and part of the fluorescein sodium salt are optically degraded by Pr_2S_3 nanoparticles.

MoS_2 nanoparticles are tested separately for their photodegradation impact on rhodamine B, rhodemaine 6 G and fluorescein sodium salt. It is found that MoS_2 can be selectively to degrade rhodamine B. As shown in figure 5, Bottle e, the rhodamine B solution, has shown a red color. After degraded by MoS_2 nanoparticles, its color becomes cyan. The photodegradation effect introduced by MoS_2 is evident through fluorescence study. Figure 8 presents fluorescence spectra of bottle e and f by using 480 nm light excitation. The fluorescence spectra of Bottle e show a peak at 600.72 nm. The fluorescence spectra of Bottle f present a peak at 582.6 nm. Further more, the intensity of the 600.7 nm peak is much higher than that of the 582.6 nm peak.

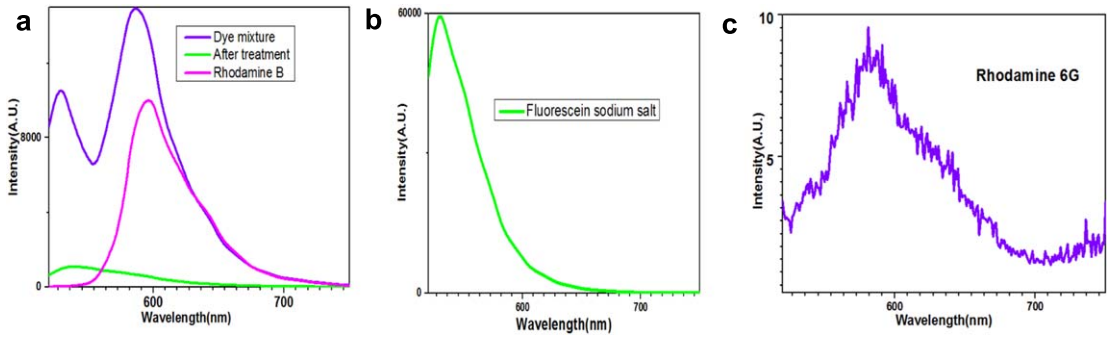

Figure 9. (a) The fluorescence spectra of the dye mixture (Dye 2) excited by 480 nm light are examined. Blue curve: no photodegradation treatment is applied; Green curve: after photodegradation treatment via MoS_2 nanoparticles; Pink curve: The fluorescence of rhodamine B excited by 480 nm light. The fluorescence spectra of fluorescein sodium salt and rhodamine 6 G excited by 480 nm are also investigated: (b) Fluorescein sodium salt; (c) Rhodamine 6 G.

MoS_2 is tested for photodegradation of the dye mixture (Dye 2). As shown in figure 5, the original color of Dye 2 is light red (see Bottle g in figure 5). After degraded by MoS_2, its color is light yellow (see Bottle h in figure 5). Figure 9 shows fluorescence investigation of the dyes and their mixture upon 480 nm light excitation. Fluorescence spectra of rhodamine 6 G, rhodamine B and fluorescein sodium salt reveal a peak at 580.9 nm, 596.6 nm and 530.2 nm, respectively. Fluorescence spectra of the mixture (Dye 2) depict two peaks at 529.3 nm and 580.6 nm. After degraded by MoS_2, it shows one peak at 538.7 nm. The intensity of the 538.7 nm peak is much lower than that of the 530.23 nm peak generated by fluorescein sodium salt. The 596.58 nm peak generated by rhodamine B is totally eliminated. Therefore, it indicates that part of fluorescein sodium salt and most of rhodamine B are degraded by MoS_2. Since the intensity of the 580.9 nm peak generated by rhodamine 6 G is very weak, it is hard to tell whether rhodamine 6 G is degraded or not.

Taking the above into account, several facts can be considered: (a) Pr_2S_3 can be applied for selective photodegradation of fluorescein sodium salt. (b) MoS_2 can be used for selective photodegradation of rhodamine B. (c) In the mixture of rhodamine B, fluorescein sodium salt and rhodamine 6 G, most of rhodamine B and part of fluorescein sodium salt are optically degraded by Pr_2S_3 nanoparticles. (d) In the mixture of rhodamine B, fluorescein sodium salt and rhodamine 6 G, part of fluorescein sodium salt and most of rhodamine B is degraded by MoS_2.

3.4. Deep-tissue imaging

A Bacon meat model is used for demonstration of the deep-tissue imaging. A 2 ml centrifuge tube is filled with Pr_2S_3 or MoS_2 nanoparticles in ethanol solution for the study of deep-tissue imaging. The nanoparticles can emit NIR fluorescence covering from 800 nm to 1100 nm upon 785 nm light excitation. Therefore, the images of the tube can be captured by a NIR camera.

Even the tube is covered by several layers of Bacon meat, part of the NIR fluorescence can still travel through the Bacon meat and reach the NIR camera. This generates the images of the tube.

Figure 10(a) is a control image captured via a 2 ml centrifuge tube which is filled with Pr_2S_3 solution. When it is covered by 1 layer of Bacon meat, the shape of the very sharp edge of the tube can be seen (see figure 10(b)). As shown in figure 10(c), when 2 layers of Bacon meat are used, the image is blurred. Finally, when 5 layers of Bacon meat are applied, the shape and edge of the tube could still be identified (see figure 10(f)). The result of using MoS_2 for deep-tissue imaging is similar (see figures 11(a)–(f)). The total thickness of 5 layers of Bacon meat is 1 cm, which indicates that the imaging depth of 1 cm is obtained.

Figure 12(a) depicts the corresponding fluorescence spectra of Pr_2S_3 solution filled 2 ml centrifuge tube after covering with various layers of Bacon meat. It can be seen that the intensity of the 808 nm peak drops when the layer thickness increases (see figure 12(b)).

Figure 13(a) presents the corresponding fluorescence spectra of MoS_2 filled 2 ml centrifuge tube after covering with various layers of Bacon meat. The intensity of the 808 nm peak decreases when the layer thickness increases (see figure 13(b)). Here, due to the limit and resolution of our instrument, the data about the fluorescence spectra and peak intensity of MoS_2 filled 2 ml centrifuge tube after covering with 5 layers of Bacon meat is absent.

Optical coherence tomography (OCT) is generally applied in clinic practices when deep tissue imaging is required. Yet it has shown a very resctricted imaging depth of 1–2 mm below the tissue surface. Development of new technologies or materials are in great demand for the deep tissue imaging.

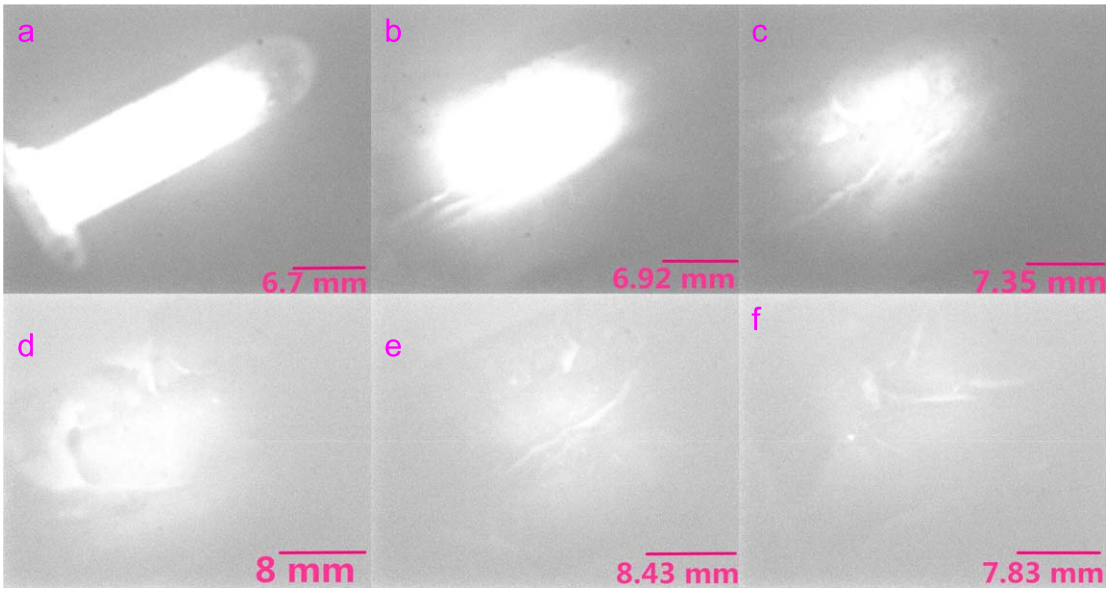

Figure 10. Deep-tissue imaging of Pr_2S_3 nanoparticles is demonstrated, using a nanoparticle-loaded 2 mL centrifuge tube covered with pig Bacon meat. (a) Control image is captured via a 2 mL centrifuge tube filled with Pr_2S_3 solution. The NIR image of the tube under multi-layers of Bacon meat is captured: (b) 1 layer; (c) 2 layers; (d) 3 layers; (e) 4 layers; (f) 5 layers. Even covered by 5 layers of the Bacon meat whose total thickness is 1 cm, we can still see the shape and edge of the tube.

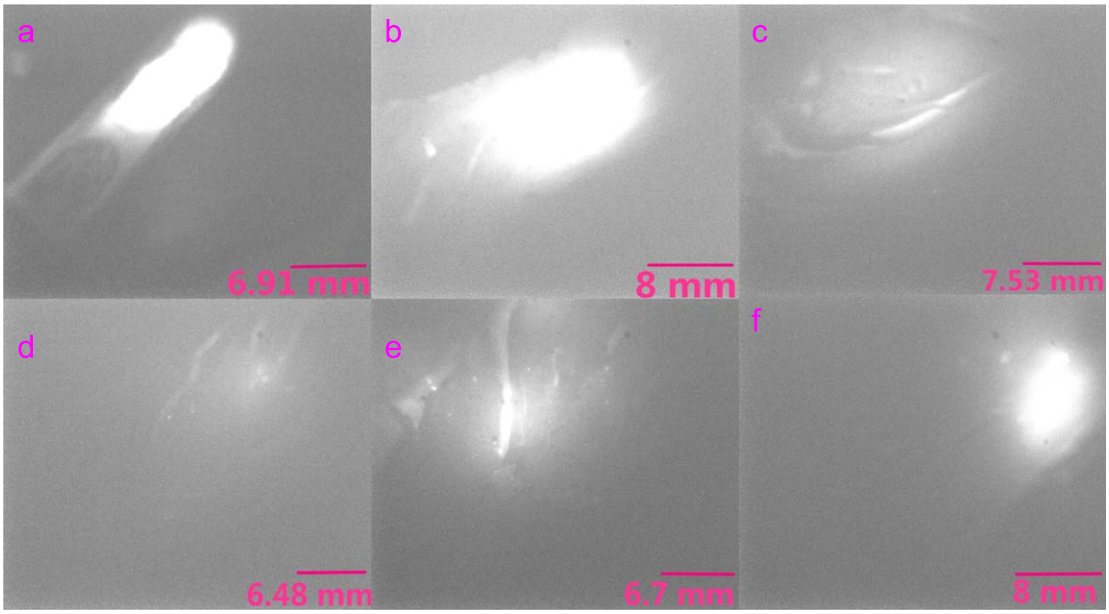

Figure 11. Deep-tissue imaging of MoS_2 nanoparticles is demonstrated, using a nanoparticle-loaded 2 mL centrifuge tube covered with pig Bacon meat. (a) Control image is captured via a 2 mL centrifuge tube filled with MoS_2 solution. The NIR image of the tube under multi-layers of Bacon meat is captured: (b) 1 layer; (c) 2 layers; (d) 3 layers; (e) 4 layers; (f) 5 layers. Even covered by 5 layers of the Bacon meat whose total thickness is 1 cm, we can still see the shape and edge of the tube.

Our NIR fluorescence imaging strategy combined with the synthesized nanoparticles is able to acheve the imaging depth of 1 cm. It can be noted that the potential application of these nanoparticles in NIR deep-tissue imaging is tremendous. They are envisioned to be used as active image contract agents in bio-medical imaging systems. Our future endevour can be focused on their combination with endoscopes or optical fiber bundles, which can be useful in dental surgical operation. They enable the remote measurement of the morphology of the dental tissue. Or our future work can be continuing to use these materials for testing their ability in dual modes tumor tissue imaging by combing magnetic sensitive materials and using animal model [23, 24].

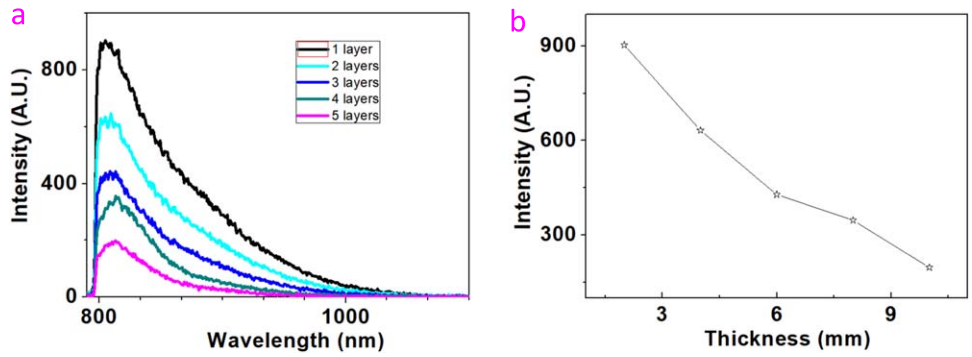

Figure 12. (a) Near-infrared fluorescence spectra of Pr_2S_3 filled 2 ml centrifuge tube after covering with various layers of Bacon meat. (b) The fluorescence peak intensity versus thickness of the Bacon meat.

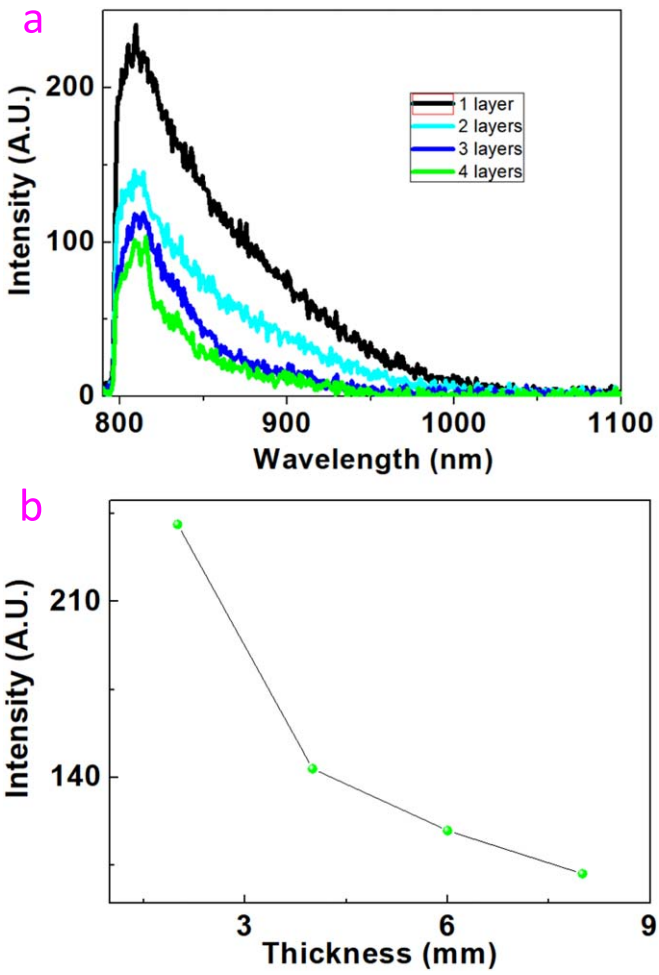

Figure 13. (a) Near-infrared fluorescence spectra of MoS_2 filled 2 ml centrifuge tube after covering with various layers of Bacon meat. (b) The fluorescence peak intensity versus thickness of the Bacon meat.

4. Conclusion

Two types of nanoparticles (Pr_2S_3 and MoS_2) were synthesized. XRD, XPS, TEM, UV–vis-NIR spectroscopy and photoluminescence spectroscopy were applied to find out their structural, morphological and optical properties. They present polychromatic-photoluminescence upon the 280 nm, 380 nm, 480 nm, 580 nm and 785 nm light excitation. Pr_2S_3 can be used for selective photodegradation of fluorescein sodium salt. MoS_2 can be utilized for selective photodegradation of rhodamine B. In the mixture of rhodamine B, fluorescein sodium salt and rhodamine 6 G, most of rhodamine B and part of fluorescein sodium salt are optically degraded by

Pr_2S_3. In the mixture of rhodamine B, fluorescein sodium salt and rhodamine 6 G, part of fluorescein sodium salt and most of rhodamine B is degraded by MoS_2. They emit NIR fluorescence (800–1100 nm) when excited by the light of 785 nm. They can be used for NIR deep-tissue imaging. Maximum imaging depth below the tissue surface of 1 cm can be achieved. Our methodology of making these nanoparticles relies heavily on a solution synthesis approach. It may be cheaply and easily to be used in industry, where the normal hydrothermal synthesis that used autoclaves can lead to high cost of fabrication. This study demonstrates the fabrication of the nanoparticles for dual applications in dye-photodegradation and NIR deep-tissue imaging.

Acknowledgments

The help from Ms Ying Xiao in Share Instruments Facility-Louisiana State University, Mr Kai Zhou in Instruments centers-Chongqing University and Dr Hao Fu from Mcgill University is appreciated. The financial support from the following agents is very appreciated: China National Key R&D Program (2017YFB1103202), Jiangsu State R&D Program(BE2018010), Key Program Special Fund in XJTLU (KSF-E-39), XJTLU Research Development Fund (RDF-18–02–20). Chongqing Research Program of Basic Research and Frontier Technology (No. cstc2017jcyjAX0469), LSU Leveraging Innovation for Technology Transfer (LIFT2) Grant: LSU-2019-LIFT-003, Louisiana Research Competitiveness Subprogram(RCS), Board of Regents Support Fund (BoRSF): LEQSF (2018-21)-RD-A-09 and LSU Biomedical Collaborative Research Program (008481).

ORCID iDs

Ye Wu https://orcid.org/0000-0002-4831-9729
Pengfei Ou https://orcid.org/0000-0002-3630-0385
Jian Xu https://orcid.org/0000-0001-6962-5146

References

[1] Wu J, Liu Q, Gao P and Zhu Z 2011 Influence of praseodymium and nitrogen co-doping on the photocatalytic activity of TiO_2 *Mat. Res. Bulletin.* **46** 1997–2003
[2] Qin C, Li Z, Chen G, Zhao Y and Lin T 2015 Fabrication and visible-light photocatalytic behavior of perovskite praseodymium ferrite porous nanotubes *J. Pow. Sour.* **285** 178–84
[3] Zinatloo-Ajabshir S and Salavati-Niasari M 2015 Nanocrystalline Pr_6O_{11}: synthesis, characterization, optical and photocatalytic properties *New J. Chem.* **39** 3948–55
[4] Xu W, Zhou G, Fang J, Liu Z, Chen Y and Cen C 2013 Synthesis and characterization of pyrochlore $Bi_2Sn_2O_7$ doping with praseodymium by hydrothermal method and its photocatalytic activity study *Inter. J. Photoener.* **2013** 1–9 234806
[5] Talebi R 2016 Novel praseodymium-doped copper ferrite: synthesis, characterization, and its photocatalyst application *J. Mater. Sci.: Mater. Electron.* **27** 6974–8
[6] Yang Y, Xia G–Z, Liu C, Zhang J-H and Wang L-J 2015 Effect of Li(I) and TiO_2 on the upconversion luminance of Pr:Y_2SiO_5 and its photodegradation on nitrobenzene wastewater *J. Chem.* **2015** 1–7 938073
[7] Vaiano V, Matarangolo M, Sacco O and Sannino D 2017 Photocatalytic treatment of aqueous solutions at high dye concentration using praseodymium-doped ZnO catalysts *Appl. Catal. B: Environ.* **209** 621–30
[8] Lee W P C, Wong F-H, Attenborough N K, Kong X Y, Tan L-L, Sumathi S and Chai S–P 2017 Two-dimensional bismuth oxybromide coupled with molybdenum disulphide for enhanced dye degradation using low power energy-saving light bulb *J. Environ. Manage.* **197** 63–9
[9] Wu Y, Xu M, Chen X, Yang S, Wu H, Pan J and Xiong X 2016 CTAB-assisted synthesis of novel ultrathin $MoSe_2$ nanosheets perpendicular to graphene for the adsorption and photodegradation of organic dyes under visible light *Nanoscale.* **8** 440–50
[10] Chen Y, Lu C, Xu L, Ma Y, Hou W and Zhu J-J 2010 Single-crystalline orthorhombic molybdenum oxide nanobelts: synthesis and photocatalytic properties *Cryst. Eng. Comm.* **12** 3740–7
[11] Xu J, Kooby D, Kairdolf B and Nie S 2017 New horizons in intraoperative diagnostics of cancer in image and spectroscopy guided pancreatic cancer surgery *New Horiz. Clinic. Case Rep.* **1** 2
[12] Xu J, Kooby D and Nie S 2018 Nanofluorophore assisted fluorescence image-guided cancer *Surgery J. Med. - Clinic. Res. & Rev.* **2** 1–3
[13] Li Z, Yao S, Xu J, Wu Y, Li C and He Z 2018 Endoscopic Near-Infrared Dental Imaging with Indocyanine *Green: a Pilot Study Ann. New York Acad. Sci.* **1421** 88–96
[14] Wu Y, Lin Y and Xu J 2019 Synthesis of Ag-Ho, Ag-Sm, Ag-Zn, Ag-Cu, Ag-Cs, Ag-Zr, Ag-Er, Ag-Y and Ag-Co metal organic nanoparticles for UV–vis-NIR wide-range bio-tissue imaging *Photochem. & Photobio. Sci.* **18** 1081–91
[15] Wong N, Kam S, O'Connell M, Wisdom J A and Dai H 2005 Carbon nanotubes as multifunctional biological transporters and near-infrared agents for selective cancer cell destruction *PNAS* **102** 11600–5
[16] Li Z, Zaid W, Hartzler T, Ramos A, Osborn M, Li Y, Yao S and Xu J 2019 Indocyanine green-assisted dental imaging in the first and second near-infrared windows as compared with X-ray imaging *Ann. New York Aca. Sci.* **1448** 42–51
[17] Lutkehoff S, Neumann M and Slebarski A 1995 3d and 4d x-ray-photoelectron spectra of Pr under gradual oxidation *Phys. Rev. B* **52** 13808–11
[18] Ogasawara H, Kotani A, Potze R, Sawatzky G A and Thole B T 1991 Praseodymium 3d- and 4d-core photoemission spectra of Pr_2O_3 *Phys. Rev. B* **44** 5465–9
[19] Kelemen S R, George G N and Gorbaty M L Direct determination and quantification of sulphur forms in heavy petroleum and coals: 1. The X-ray photoelectron spectroscopy (XPS) approach *FUEL.* **69** 939–44

[20] Pashutski A and Folman M 1989 Low temperature XPS studies of NO and N_2O adsorption on Al(100) *Surf. Sci.* **216** 395–408
[21] Sheng Z-H, Shao L, Chen J-J, Bao W-J, Wang F-B and Xia X–H 2011 Catalyst-free synthesis of nitrogen-doped graphene via thermal annealing graphite oxide with melamine and its excellent electrocatalysis *ACS Nano* 4350–8
[22] Choi J-G and Thompson L T 1996 XPS study of as-prepared and reduced molybdenum oxides *Appl. Surf. Sci.* **93** 143–9
[23] Li Y, Tang J, He L, Liu Y, Liu Y, Chen C and Tang Z 2015 Core–shell upconversion nanoparticle@metal-organic framework nanoprobes for luminescent/magnetic dual-mode targeted imaging *Adv. Mat.* **27** 4075–80
[24] Hou K, Fixler D, Han B, Shi L, Feder I, Duadi H, Wang X and Tang Z 2017 Towads *in vivo* tumor detection using polarization and wavelength characteristics of self-assembled gold nanorods *Chem. Nano. Mat.* **3** 736–9